

Flux pinning by $\text{Nd}_4\text{Ba}_2\text{Cu}_2\text{O}_{10}$ inclusions in $\text{NdBa}_2\text{Cu}_3\text{O}_{7-\delta}$ superconductors: A combined effect of point, interface, and $\Delta\kappa$ pinning at elevated temperatures

Tadashi Mochida, Noriko Chikumoto, and Masato Murakami

Superconductivity Research Laboratory, International Superconductivity Technology Center, 1-16-25, Shibaura, Minato-ku, Tokyo 105-0023, Japan

(Received 31 January 2000; revised manuscript received 6 April 2000)

We have systematically studied the role of $\text{Nd}_4\text{Ba}_2\text{Cu}_2\text{O}_{10}$ (Nd422) nonsuperconducting inclusions for flux pinning in oxygen-controlled-melt-growth processed Nd-Ba-Cu-O bulk superconductors. Nd422 inclusions act as interface pinning which is the most dominant in low-field and high-temperature region. In addition, they are also effective in enhancing the critical current density (J_c) even in a high-field region and thus the irreversibility field (B_{irr}). Three pinning regimes have been identified at elevated temperatures ($T \geq 77$ K): a combination of point and interface pinning in low fields; a combination of interface and $\Delta\kappa$ pinning in intermediate fields; and interface pinning with a slight influence from $\Delta\kappa$ pinning in high fields. Nd422 addition shifted the boundary of the pinning regime to higher fields. We have found overall J_c is almost a simple summation of two contributions: interface pinning and $\Delta\kappa$ pinning.

I. INTRODUCTION

Large critical current density (J_c), high irreversibility field (B_{irr}), and small magnetic relaxation are required for power applications of high-temperature superconductors.¹ Up to now, R -Ba-Cu-O bulk superconductors (R : rare earth elements) are the most promising candidates for high-field applications. Melt-processing² has been employed successfully to the fabrication of R -Ba-Cu-O bulk superconductors which exhibit large J_c values even at elevated temperatures. The key to attaining high J_c is the introduction of effective pinning centers without decaying the matrix superconducting properties.

Melt-processed R -Ba-Cu-O bulks contain various defects such as nonsuperconducting second-phase precipitates, twin boundaries, point defects (oxygen vacancies), stacking faults, and dislocations, which all may serve as pinning centers. For bulk R -Ba-Cu-O fine dispersion of $R_2\text{BaCuO}_5$ ($R211$) particles into a $R123$ matrix is effective in enhancing pinning, which led to J_c enhancement to the level of 10^9 A/m² at 77 K.³

Nd-Ba-Cu-O is a promising alternative to Y-Ba-Cu-O because of its high T_c and large J_c at high magnetic fields. A large growth rate is also an attracting feature for commercial mass production.⁴ In an early stage of development, however, Nd-Ba-Cu-O showed poor superconducting properties when melt-processed in air.^{5,6} Unlike the Y-Ba-Cu-O, which forms only a stoichiometric $\text{YBa}_2\text{Cu}_3\text{O}_y$ (Y123), the Nd-Ba-Cu-O system forms a $\text{Nd}_{1+x}\text{Ba}_{2-x}\text{Cu}_3\text{O}_y$ type solid solution (Nd123ss) (Refs. 5 and 7) and a large amount of Nd ions substitute for Ba when melt-processed in air. This results in a depression of the carrier concentration and thus lower T_c .⁷ Later it was found that such Nd-Ba substitution can largely be suppressed when the samples were melt-processed in a reduced oxygen atmosphere, which is the oxygen-controlled-melt-growth (OCMG) process.^{6,8} The OCMG-processed Nd-Ba-Cu-O samples show a sharp superconducting transition with a high onset T_c of 96 K.⁹ In addition, they exhibit a secondary peak effect in the J_c - B curve, which

suppressed the decay of J_c values even in a high-field region.

The secondary peak effect has also been observed in R -Ba-Cu-O systems with no R -Ba substitution.¹⁰ In this case, however, the peak effect originates from local oxygen-deficient regions or weak-superconducting regions caused by chemical contamination.^{11,12} This is supported by the fact that the peak effect was not observed in fully oxygenated ultrapure Y123 single crystals grown in a BaZrO_3 crucible.¹³ Murakami *et al.*⁸ proposed that the presence of Nd-rich Nd123ss clusters might be responsible for the peak effect in the Nd-Ba-Cu-O system. Later Egi *et al.*¹⁴ and Wu Ting *et al.*¹⁵ confirmed that Nd123 single crystals contain small clusters of 10–50 nm diameter, which have Nd content slightly higher than that of the Nd123 matrix. Such compositional fluctuation will cause spatial variation of the Ginzburg-Landau parameter ($\kappa = \lambda/\xi$) or T_c , which then provides additional flux pinning ($\Delta\kappa$ pinning^{16–19} or δT_c pinning^{20–22}). Chikumoto *et al.*²³ showed that the peak effect in Nd-Ba-Cu-O disappeared when compositional fluctuation in the matrix was annihilated with high-temperature annealing, which supports the fact that the peak effect is caused by the presence of Nd-rich Nd123ss clusters. For some R -Ba-Cu-O bulk materials, however, oxygen-deficient regions or chemically contaminated regions are also present depending on the processing conditions.²⁴ Furthermore, the optimum oxygen-annealing conditions are dependent on the x value of $\text{Nd}_{1+x}\text{Ba}_{2-x}\text{Cu}_3\text{O}_y$.²⁵ Thus, the function of Nd123ss clusters as pinning centers is also dependent on the oxygenation levels of both the matrix and the clusters. In addition, the presence of other defects, such as intermediate precipitate structure²⁶ and three-dimensional dislocations,²⁷ has been reported in melt-processed Nd-Ba-Cu-O. Such complexity should be taken into consideration for understanding the pinning mechanism in Nd-Ba-Cu-O superconductors.

For further development of high-performance R -Ba-Cu-O bulk superconductors, it is important to identify the dominant pinning center. It is also interesting to study mutual interaction of various pinning centers such as Nd422/Nd123 inter-

face pinning and $\Delta\kappa$ pinning. In this paper, we focused on the function of Nd422 inclusions as pinning centers, since the size and volume of Nd422 are controllable. We prepared several Nd123/Nd422 composite bulk samples with various amounts of Nd422 particles in different sizes. Special care was also paid to controlling the oxygenation level of the Nd123 matrix to be constant, since the oxygen deficiency strongly affects the superconducting properties.²⁴ We measured the J_c values, the irreversibility fields, and the volume pinning force for Nd123/Nd422 composite samples and Nd123 single crystals with the aim of clarifying the function of Nd422 particles.

II. EXPERIMENTAL

A $\text{NdBa}_2\text{Cu}_3\text{O}_{7-\delta}$ single crystal (sample FSC) was grown by a flux growth method in an yttria-stabilized zirconia crucible using the flux composition of $\text{Nd}:\text{Ba}:\text{Cu}=2:30:68$ in flowing 0.1% O_2/Ar mixture gas, the details of which are described in Ref. 28. Nd-Ba-Cu-O bulk samples were prepared by the following procedures. Commercial powders of Nd123, Nd422, Pt, and CeO_2 were used as precursors. Samples MT1, MT2, and MT3 were prepared using powders of Nd123 and Nd422, while Pt and CeO_2 were added to the sample MT1F in order to refine the size of Nd422. The nominal compositions are Nd123 + 10 mol % Nd422 (MT1), Nd123 + 20 mol % Nd422 (MT2), Nd123 + 30 mol % Nd422 (MT3), and Nd123 + 10 mol % Nd422 + 0.5 wt % Pt + 1.0 wt % CeO_2 (MT1F). The powders were well grounded and pressed into pellets, which are subsequently subjected to cold isostatic pressing. Consolidated pellets were subjected to the OCMG process in flowing O_2/Ar mixture gas. The detailed sample preparation methods for MT1, MT2, and MT3 are described in Ref. 29 and that for MT1F is in Ref. 30. Here all the samples were grown under the same oxygen partial pressure of 0.1% and fully oxygenated at 300 °C (Ref. 31) for 150 h to minimize the variation of x and δ in the $\text{Nd}_{1+x}\text{Ba}_{2-x}\text{Cu}_3\text{O}_{7-\delta}$ matrix.

Microstructural observations were performed with a scanning electron microscope (SEM). The size and the volume fraction of Nd422 particles trapped in the Nd123 matrix were estimated using an image analyzer. The average particle size of Nd422 was determined on the assumption that the Nd422 particles are spherical. The volume fraction was deduced from the total area of Nd422 particles in a SEM micrograph.²⁹ Figure 1 shows SEM micrographs of the OCMG-processed Nd-Ba-Cu-O samples. The volume fraction V_f and the average diameter d of Nd422 are summarized in Table I. It should be noted that Nd422 particles are drastically refined with a combined addition of Pt and CeO_2 .³⁰

Magnetization measurements were carried out using a Quantum Design superconducting quantum interference device (SQUID) magnetometer (MPMS-7) with magnetic fields applied parallel to the c axis. The critical temperature (T_c) is determined by measuring the temperature dependence of the dc magnetic moment in an applied field of 1 mT. Data acquisition was performed 30 s after reaching the target temperature. All the samples show onset T_c 's above 93.8 K and a sharp superconducting transition width within 1.5 K (Table I). According to Takita *et al.*,³² the T_c higher than 93 K indicates that x in the formula $\text{Nd}_{1+x}\text{Ba}_{2-x}\text{Cu}_3\text{O}_y$

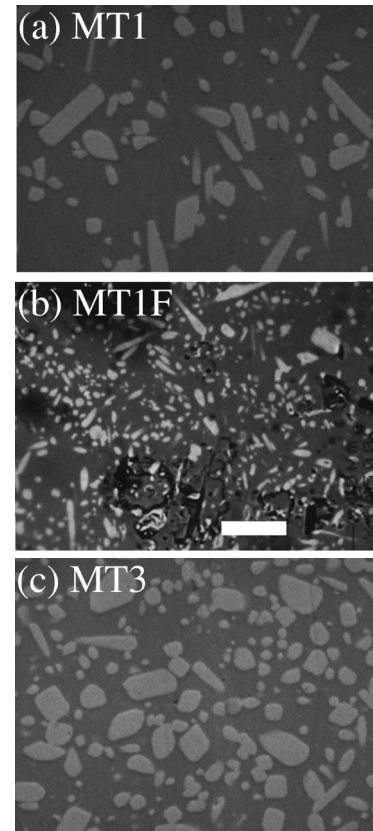


FIG. 1. SEM micrograph of the OCMG-processed samples for (a) MT1 (Nd123 + 10 mol % Nd422), (b) MT1F (Nd123 + 10 mol % Nd422 + 0.5 wt % Pt + 1.0 wt % CeO_2), and (c) MT3 (Nd123 + 30 mol % Nd422). The average diameters of second-phase particles for MT1 and MT2 are about 2 μm while that for MT1F is drastically reduced to about 1.2 μm . The scale bar represents 10 μm .

is smaller than 0.05. None of the samples showed any step or plateau in the superconducting transition, which demonstrates that the samples consist of a single superconducting phase. The high- and similar T_c values indicate that all of the samples are fully oxygenated.

Magnetization hysteresis curves were measured in a persistent current mode with a scan length of 30 mm. Data acquisition was performed 30 s after reaching the target field, and the three data were averaged. As a result, it took 90 min to measure a quarter-loop from 0 to 7 T (≈ 1.3 mT/s). The true irreversible component of magnetization is deduced by subtracting the background from the measured signal. The J_c values were calculated using the extended Bean model³³ from the irreversible magnetization.

III. RESULTS AND DISCUSSION

A. Critical currents and irreversibility fields

Figure 2 shows semilogarithmic plots of J_c versus temperature for both single-crystal and OCMG-processed Nd-Ba-Cu-O samples. In the low-temperature region below 60 K, it shows a quasiexponential relationship of $J_c \propto \exp(-CT)$, where C is a constant. Such dependency is also observed in other R-Ba-Cu-O.³⁴ According to Higuchi, Yoo, and Murakami,³⁵ such temperature dependence can be ex-

TABLE I. The list of the Nd-Ba-Cu-O samples used in this study.

Sample	Sample size (mm)			T_c (K) onset	V_f	d $\times 10^{-6}$ m	V_f/d $\times 10^5$ m $^{-1}$
	a	b	c				
FSC	0.63	0.79	0.08	93.8	0.00	—	0.0
MT1	1.75	1.94	0.69	94.5	0.19	1.9	1.0
MT1F	1.46	1.54	0.32	94.5	0.18	1.2	1.5
MT2	1.55	1.60	0.64	94.5	0.25	1.8	1.4
MT3	1.23	1.49	0.62	95.0	0.34	1.7	2.0

plained by the collective creep model (CC model)^{20,21,36,37} by taking account of the flux creep effect. This suggests that weak pinning (e.g., point defects) typical for the CC model is active in a low-temperature region. This is also supported by the fact that J_c values of FSC (which contains no Nd422 inclusions) are larger than those of melt-processed Nd-Ba-Cu-O samples at low temperatures. On the other hand, a large deviation from the exponential relation is observed at $T > 60$ K. This suggests the weak pinning assumed in the CC

model is not active at high temperatures. According to Martínez *et al.*,³⁸ the temperature where the deviation occurs from the relation $J_c \propto \exp(-CT)$ corresponds to a depinning line of point defects. It is thus expected that strong pinning (Nd422 inclusions) plays an important role at high temperatures. Hence J_c values are governed by the volume fraction of Nd123 matrix.

Based on the core pinning model, Murakami *et al.*³⁹ proposed that the pinning energy should be proportional to the interface area of Y123/Y211, which is represented by V_f/d . This type of pinning is called interface pinning, since the origin of the pinning energy is the difference in the condensation energy at the interface between superconducting and normal regions. In fact, many experimental results have confirmed that J_c is increased with increasing V_f/d in Y-Ba-Cu-O.^{3,38,40,41} The present results indicate that the zero-field J_c values are larger than those at the peak fields in the OCMG-processed samples, which is observed at temperatures above 60 K. This is the most prominent for sample MT3 which has the largest V_f/d value, while it is not observed in FSC with no Nd422 inclusions. These results indicate that an increase in V_f/d value leads to J_c enhancement like the case of Y211 in melt-processed Y-Ba-Cu-O.

In Nd-Ba-Cu-O system, however, opinions vary as to the effectiveness of Nd422 inclusions. For example, Yu *et al.*⁴² argued that flux pinning by Nd422 would not be so effective as Y211 on the basis of J_c - T curves and TEM observations of Nd123/Nd422 interfaces. However, the present results indicate that the J_c values of the OCMG-processed samples are larger than those of FSC at temperatures above 60 K. Here we note that J_c values in the present Nd-Ba-Cu-O samples are as high as those of Y-Ba-Cu-O reported by Martínez *et al.*³⁸ and Higuchi, Yoo, and Murakami.³⁵ In addition, J_c - T curves are strongly sample dependent such that J_c values increase either by increasing Nd422 contents (MT2 and MT3) or reducing Nd422 size (MT1F). It is also notable that the J_c values decay rapidly in FSC, while the decay is smaller for the OCMG-processed samples with larger V_f/d values. These results indicate that Nd422 addition is effective in enhancing J_c values for the Nd-Ba-Cu-O system, especially in a low-field and high-temperature region.

Figure 3 shows plots of J_c - B curves for the present samples at temperatures above 77 K. A decrease in J_c with B at lower fields and fishtail peaks in an intermediate-field range are observed in all the samples. There is a small trough or a deflection (B^{defl} , J_c^{defl}) in J_c - B curve at fields below 1 T, which may be a crossover from the field region, where the interface pinning is dominant, to the field region, where the fishtail peak is observed. It is also notable that the deflection

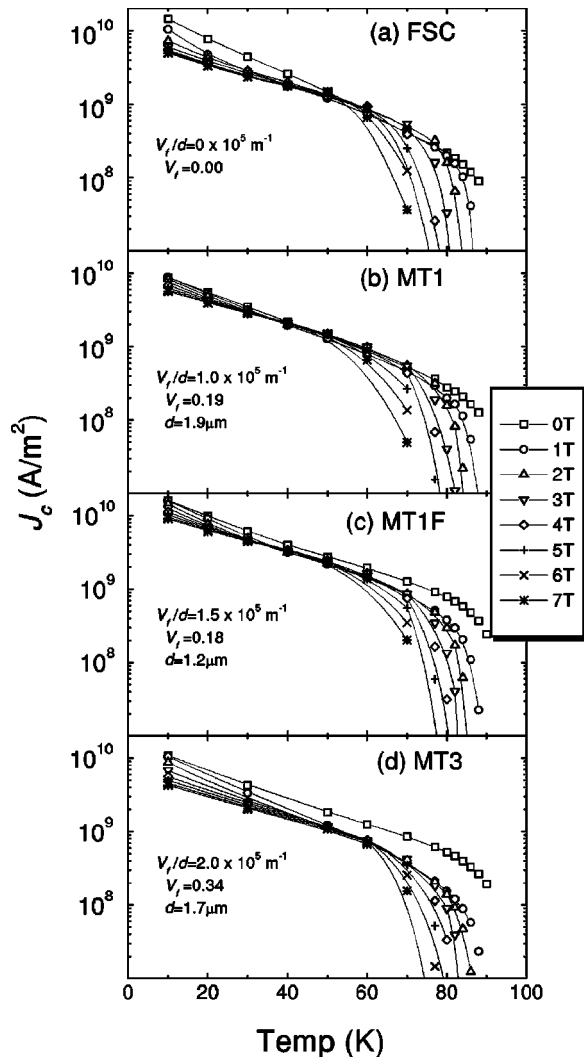


FIG. 2. The temperature dependence of J_c ($H \parallel c$) for (a) FSC, (b) MT1, (c) MT1F, and (d) MT3 at various fields. Note that the J_c at self-field is the largest above 60 K and that abrupt decrease in J_c is prominent above 70 K.

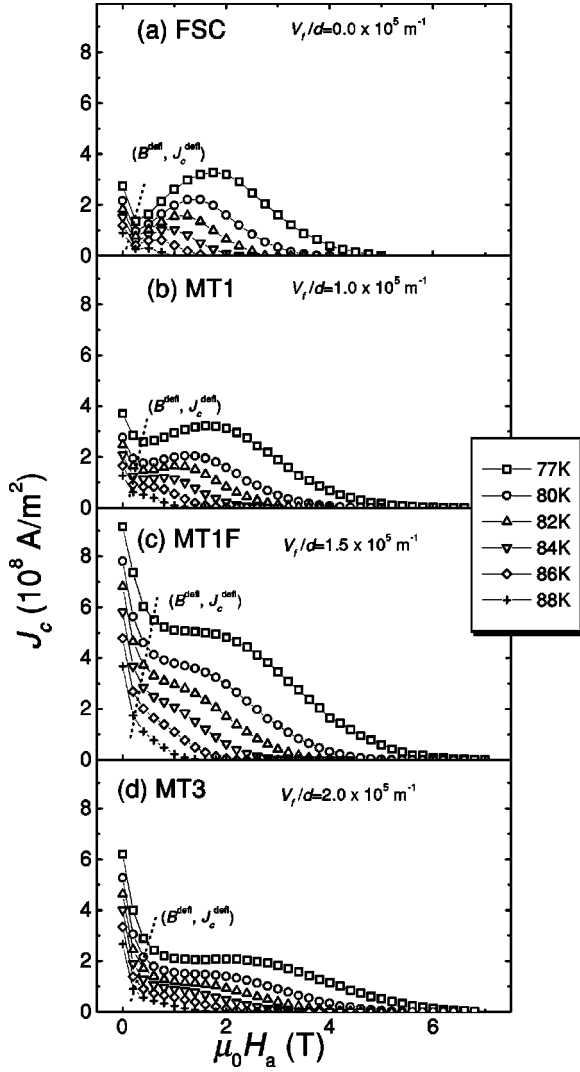


FIG. 3. The field dependence of $J_c(H||c)$ at temperatures above 77 K for the samples with various amounts of Nd422 particles in different size: (a) FSC, (b) MT1, (c) MT1F, and (d) MT3. The deflection (B^{defl}, J_c^{defl}) is represented by a dotted line in the figure. Note that reducing the Nd422 size is very effective for increasing J_c near zero field. The secondary peak is the most prominent for the single crystal while it smears out with increasing Nd422 content.

is less evident with increasing temperature. The peak effect is the most prominent for FSC and is smeared with increasing Nd422 content. At fields above 3 T, a small increase in J_c is seen for the samples with Nd422 addition.

Figure 4 shows the field dependence of J_c normalized by the J_c value at $B = 0$ T ($J_c/J_{c,B=0}$) to enlighten the relation between the interface pinning and the fishtail effect. The fishtail is clearly observed in FSC with $J_c/J_{c,B=0} \approx 1.3$ at the peak. On the other hand, the fishtail is smeared with increasing Nd422 content, and $J_c/J_{c,B=0} \approx 0.35$ for MT3, resulting in a plateaulike J_c - B curve instead of a clear peak. A large difference in J_c values at the peak field suggests that the pinning mechanism is different from that dominant at $B = 0$. An interesting feature is that the fishtail shape is not so prominent for MT1F in comparison with MT1 despite the fact that both samples have similar V_f/d values, which will be treated in Sec. III C. It is also important to note that the value of $J_c/J_{c,B=0}$ for all the samples merge into a single

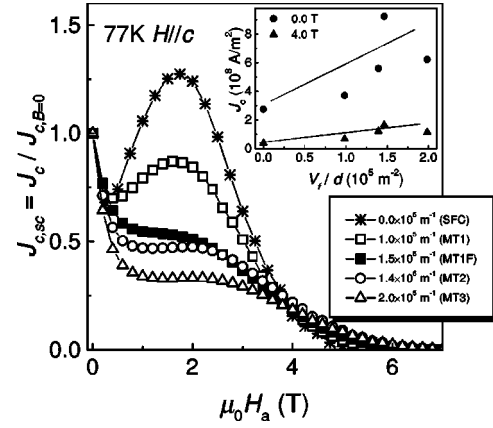


FIG. 4. The field dependence of $J_c(H||c)$ at 77 K for the samples studied here. The J_c value is scaled by the value at self-field ($J_{c,sc} \equiv J_c/J_{c,B=0}$). Inset: the J_c values at self-field and 4 T are plotted as a function of V_f/d , showing the linear relation between J_c and V_f/d .

line at fields above 4 T, which implies that the pinning mechanism in a higher-field region has a close relation with that in low fields, i.e., Nd123/Nd422 interface pinning.

The inset of Fig. 4 shows the relationship between J_c and V_f/d at 77 K. It is clear that the J_c values are proportional to V_f/d , both in the remnant field and at 4 T. This supports the fact that nonsuperconducting Nd422 inclusions are effective pinning centers both at low and high fields, where field-induced pinning is not active.

Here, we note that the effect of twins is not important in the present samples. It is known that twins may cause an additional intermediate peak in J_c - B curves at elevated temperatures.⁴³ However, none of our samples showed any additional peak. This indicates the effects of twins are negligible in the present study.

Next, we see the effect of Nd422 inclusions on the irreversibility field (B_{irr}), which was obtained from the magnetization measurements using a current-density criterion of 10^6 A/m². The first important point to note is that the Nd-Ba-Cu-O samples exhibit the B_{irr} of about 7 T at 77 K when measured with a SQUID magnetometer at a sweep rate of 1.3 mT/s. This indicates that a high B_{irr} can be achieved even in the sample with a large amount of Nd422 inclusions, in contrast to a conventional expectation.²⁴ Furthermore Nd422 inclusions can enhance both J_c in a high-field region and B_{irr} . Thus it is expected that both high B_{irr} and large J_c can be achieved by further optimizing the size and contents of Nd422 inclusions.

Figure 5 shows the irreversibility lines (IL's) for the samples. Although all the samples show similar T_c ranging from 93.8 to 95.0 K, the irreversibility line is strongly sample dependent. It is known that a different oxygen content affects the IL,²⁴ however, similar T_c values among the samples indicate that the Nd422 inclusions are mainly responsible for the difference. The IL shifts to higher fields with increasing Nd422 content, indicating that Nd422 inclusions are effective in enhancing the IL. These results are consistent with the result that J_c values in a high-field region are increased with increasing V_f/d . An enhancement in B_{irr} by adding secondary inclusions can also be seen in other references both in Y-Ba-Cu-O (Refs. 3, 40, and 44 and more

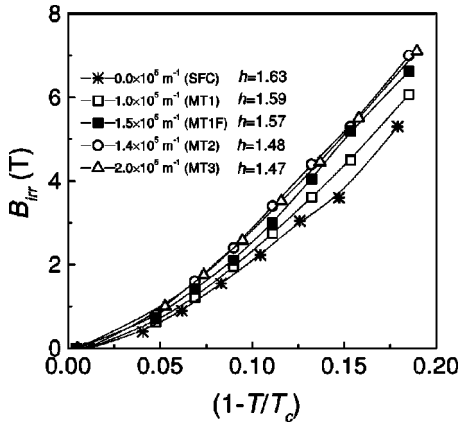


FIG. 5. The irreversibility line (IL) for the samples with $H||c$, plotted in reduced temperature. Note that IL shifts to higher field with increasing Nd422 content. The h value in $B_{irr}(T/T_c) = B_0[1 - T/T_c]^h$ is listed in the figure.

recently in the (Nd, Eu, Gd)-Ba-Cu-O system.⁴⁵ These results suggest that the IL is related to the secondary inclusions that govern a depinning.⁴⁶ The temperature dependence of the IL is often described by the following expression:

$$B_{irr}(T/T_c) = B_0[1 - T/T_c]^h. \quad (1)$$

The h values, deduced from the measured data using a least-square method, are listed in Fig. 5. Here, the compositional dependence is also recognized. Although the h value is very close to 1.5, it systematically decreases from 1.60 (SFC) to 1.47 (MT3) with increasing Nd422 contents. This result also supports the fact that Nd422 inclusions enhance IL's. It may be worth pointing out that the pinning mechanism that determines the IL is identical in this temperature region ($0.8 \leq t \leq 1.0$). According to Almasan *et al.*⁴⁷ and Dalichaouch *et al.*,⁴⁸ a deviation from $h \approx 3/2$ is an indication of a crossover of pinning regimes, which is observed around $t \equiv T/T_c \approx 0.6$ in Y-Ba-Cu-O. In our case also, any significant change in h was not observed in the temperature window of our experiments, which agrees well with the literature.

B. Volume pinning force F_p

Volume pinning force analysis is very useful to learn about the pinning properties. In conventional superconductors, a scaling of F_p was performed by plotting the normalized pinning force F_p/F_p^{max} versus the reduced field $b = B/B_{c2}$, where B_{c2} denotes the upper critical field.^{18,19} Thus F_p is described by

$$F_p = [B_{c2}(T)]^\beta \times f(b), \quad (2)$$

where β is a numerical fitting parameter. Here $f(b)$ is a pinning function and reflects the size and character of the defects providing the pinning based on the study of conventional pinned type-II superconductors. For various high- T_c materials, the scaling of F_p is found as well, however, experiments have shown that the appropriate scaling field is the irreversibility field B_{irr} instead of B_{c2} .^{49,50} Thus a general expression of the volume pinning force $F_p(B)$ is given in the form

TABLE II. The scaling parameters γ and δ in $F_p \propto b_{irr}^\gamma (1 - b_{irr})^\delta$ obtained from the data in the entire field region ($0 < B < B_{irr}$) at 77 K.

Sample	parameter	
	γ	δ
FSC	2.30 ± 0.08	3.09 ± 0.11
MT1	2.01 ± 0.06	3.02 ± 0.10
MT1F	1.60 ± 0.05	2.52 ± 0.08
MT2	1.72 ± 0.06	2.54 ± 0.09
MT3	1.70 ± 0.07	2.31 ± 0.09

$$F_p(b_{irr})/F_p^{max} = A b_{irr}^\gamma (1 - b_{irr})^\delta, \quad (3)$$

where A is a numerical parameter, γ and δ scaling parameters, and b_{irr} a reduced magnetic induction $b_{irr} \equiv B/B_{irr}$. The scaling parameters γ and δ for the present samples at 77 K were obtained by a least-square method and are shown in Table II. It is evident that both γ and δ are composition dependent, indicating pinning characteristics are different among the samples, which is attributed to the amount of Nd422 inclusions because γ and δ systematically decreases with increasing Nd422 content. This is also in good agreement with the results by Higuchi, Yoo, and Murakami,³⁵ who reported smaller γ and δ values for a melt-processed Y-Ba-Cu-O sample compared to those for Nd-Ba-Cu-O. In this section, the effect of Nd422 inclusions on flux pinning is further evaluated by using several scaling functions. Since J_c - B properties are classified into three field regions, we will analyze the field dependence of F_p - B properties separately in low-, intermediate- and high-field regions.

In a low-field regime where $b_{irr} \ll 1$ in Eq. (3), a power-law relation of $F_p \propto B^\gamma$ is recognized. The γ values at temperatures above 77 K for the samples are listed in Table III. The important point to note is that the γ value depends on both composition and temperature. At 77 K, for example, it decreases from 1.26 (for Nd123SC) to 0.53 (for MT3) with increasing Nd422 content, suggesting that a decrease in γ is attributed to the presence of normal second-phase particles. It is also notable that the γ value for OCMG-processed Nd-Ba-Cu-O samples decrease with increasing temperature. For example, the γ value for MT1 decreases from 0.87 to 0.77 as the temperature is raised from 77 to 86 K, whereas the γ value for the single crystal shows almost temperature-independent value ($\gamma \approx 1.2$). The most likely explanation for the composition and temperature-dependent γ is the inter-

TABLE III. The γ values in $F_p \propto B^\gamma$ at various temperatures obtained from the data in the low field region ($0 < B < 0.5$ T).

Sample	Temperature (K)					
	77	80	82	84	86	88
FSC	1.26	1.21	1.26	1.27	1.27	1.09
MT1	0.87	0.85	0.84	0.86	0.86	0.77
MT1F	0.74	0.71	0.68	0.64	0.58	0.35
MT2	0.67	0.63	0.63	0.60	0.57	0.50
MT3	0.53	0.50	0.47	0.43	0.38	0.33

play between interface pinning and other weaker pinning (e.g., oxygen defects, impurities, etc.).

According to Matsushita and co-workers,⁵¹ the relation of $F_p \propto B^{1/2}$ is expected in the case of interface pinning by non-superconducting particles, since the average diameter of the particles is larger than the coherence length ξ . This relation is deduced based on the direct summation of elementary pinning forces in a creep-free case. On the other hand, $F_{p0} \propto B$ is expected for the normal point pinning since the spacing of pinning centers is smaller than a_f and hence every vortex can interact with a pinning center, which results in the relation: $F_p \propto 1/a_f^2$. In OCMG-processed Nd-Ba-Cu-O samples, it would be reasonable to assume that both interface pinning and point pinning are active. As the temperature is raised, the contribution from point defects will be weakened with thermal fluctuation; instead Nd123/Nd422 interface pinning becomes more dominant. Thus the γ value shifts to 1/2 with increasing temperature. On the contrary, only microscopic features (e.g. cation, disorder, and oxygen defects) are expected to act as dominant pinning centers in FSC which does not contain any Nd422 particles. In fact, FSC exhibits the highest γ value of 1.26 at 77 K, which is close to the theoretical estimate of small pinning centers.¹⁸ In addition, the temperature-independent γ value shows some unique pinning dominates in the temperatures above 77 K. These results lead to the conclusion that the dominant pinning mechanism in a low-field regime is the combination of Nd123/Nd422 interface pinning and point pinning.

As the magnetic field H_a is increased, compositional fluctuation in Nd-Ba-Cu-O superconducting matrix will cause spatial variation of the Ginzburg-Landau parameter (κ). Thus, the $\Delta\kappa$ pinning is supposed to play an important role when magnetic field is increased. In fact, $\Delta\kappa$ pinning is supposed to enhance the flux pinning in an intermediate-field region, and thereby leading to an increase in J_c .^{11,52,53} According to Klein *et al.*,⁵⁰ for $\Delta\kappa$ pinning $f_p(b_{F_p})$ has the form

$$f_p(b_{F_p}) = 3b_{F_p}^2(1 - 2b_{F_p}/3), \quad (4)$$

where f_p is the scaled volume pinning force defined as $f_p = F_p/F_p^{\max}$, and b_{F_p} is the scaled field defined as $b_{F_p} = B/B_{F_p}^{\max}$. Figure 6 shows the plots of f_p versus b_{F_p} , in which a good scaling is recognized for Nd123 single-crystal and melt-processed Nd-Ba-Cu-O samples in the high-field region above $B_{F_p}^{\max}$. The deviation from a master curve observed in f_p - b_{F_p} curves at low fields is attributable to the presence of interface pinning, because it becomes more evident either with increasing temperature or Nd422 content. It is interesting to note that the f_p - b_{F_p} curve is quite similar to the theoretical calculation by Klein *et al.* for a single crystal (FSC). The curve is almost symmetric with f_p approaching zero at $b_{F_p} \approx 2.3$. In the intermediate-field region of $0.5 < b_{F_p} < 1.2$, b_{F_p} dependencies are also well described by this equation for the OCMG-processed Nd-Ba-Cu-O samples. This supports the assumption that $\Delta\kappa$ pinning is dominant in the OCMG-processed samples in the intermediate-field range like a single crystal. However, as pointed out by Klein *et al.*,⁵⁰ the scaling holds only to $B_{F_p}^{\max}$, and therefore, the

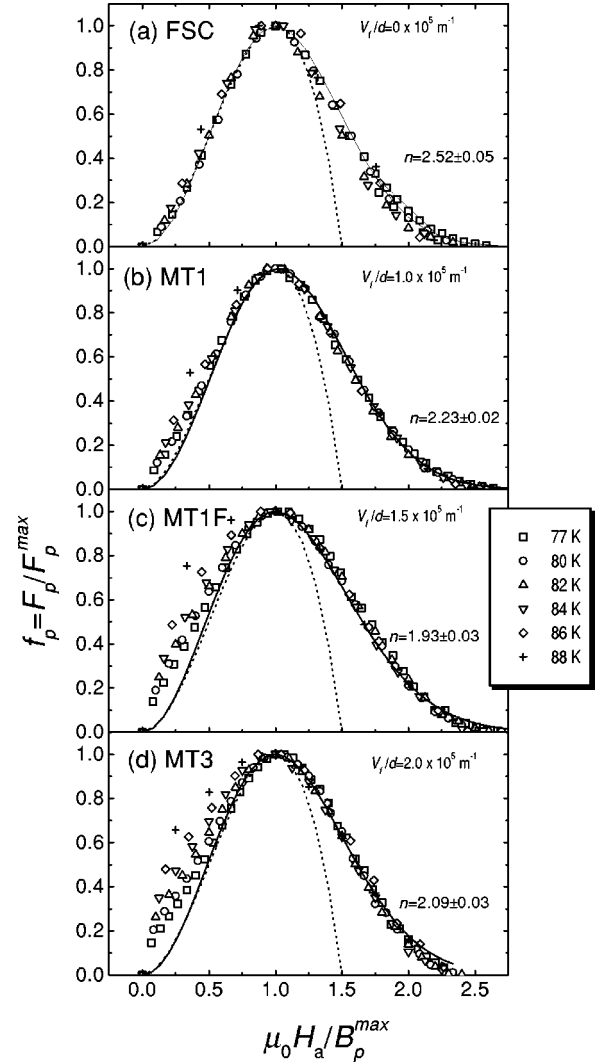


FIG. 6. The plots of $F_p/F_p^{\max} (=f_p)$ versus $B/B_{F_p}^{\max} (=b_{F_p})$ at temperatures above 77 K for (a) SFC, (b) MT1, (c) MT1F, and (d) MT3. Dashed lines correspond to the fitting by using Eq. (4), which is the theoretical model of $\Delta\kappa$ pinning by Klein *et al.* Solid lines correspond to the fitting by using Eq. (10) for the data at 77 K. The n value in Eq. (10) is also shown in the figure.

deviation from the master curve may take place at higher fields, which is observed in the present experiment, and also in Y123 single crystals with the peak effect as reported by Hyun *et al.*⁵⁴ On the other hand, a good scaling in f_p - b_{F_p} above $b_{F_p} = 1$ suggests the presence of some universal pinning mechanism that dominates the $J_c(B, T)$ behavior in this field region and also $B_{irr}(T)$.

Figure 7 shows f_p versus $b_{irr} (=B/B_{irr})$ at 77 K, which clearly enlightens the effect of Nd422 inclusions in the high-field region. A slight increase in f_p above the peak field ($B_{F_p}^{\max}$) is observed by increasing V_f/d (MT1F and MT3). The peak position also shifts to higher fields. These results imply that Nd123/Nd422 interface pinning lead to a large volume pinning force at relatively high fields.

In order to study the effect of Nd422 inclusions further, we studied the f_p - b_{irr} dependence above $B_{F_p}^{\max}$. For analyses, we used the catastrophic⁵⁵ and the avalanching depinning model⁵⁶ since these models provide information on the de-

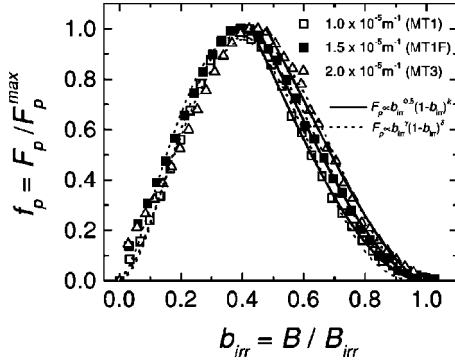


FIG. 7. The plot of $f_p - b_{irr}$ curves at 77 K for MT1, MT1F, and MT3. The solid lines correspond to the fitting by using the data above $B_{F_p}^{max}$ and the $F_p \propto b_{irr}^{1/2}(1 - b_{irr})^k$ relation. Note that the k value is affected by Nd422 inclusions and it decreases from 2.09 (MT1) to 1.68 (MT3) with increasing Nd422 content. The k value is listed in Table IV.

pinning behavior in a high-field region. In the catastrophic depinning model, pinning centers are assumed not to be strong enough to support a large driving force, and the local plastic deformation takes place, leading to a catastrophic flux flow in a sample. The model gives the following functional form:

$$F_p = \alpha_L d_i \propto C_{66} a_f \propto b^{1/2}(1 - b)^2, \quad (5)$$

where α_L is the Labusch parameter, d_i the interaction distance, C_{66} the shear moduli, a_f the flux line lattice spacing, and b is a reduced magnetic induction.

In the avalanche depinning model, pinning potentials are assumed to be deeper than those in the catastrophic model, i.e., the local plastic deformation of fluxoid can be supported by pinning centers. This model gives the following relation:

$$f_p \propto b^{1/2}(1 - b). \quad (6)$$

Thus we performed a numerical fitting using the form

$$f_p \propto b^{1/2}(1 - b)^k, \quad (7)$$

which is a special case of Eq. (3) with $b = b_{irr}$, $\gamma = 1/2$, and k the fitting parameter. Here, the data at $B_{F_p}^{max} < B$ are used for the fitting because our purpose is to investigate the effect of Nd422 in a high-field region.

The results of the numerical fitting are shown in Fig. 7 as solid lines. It is evident that the $f_p - b_{irr}$ curve is well described by the functional form of $f_p \propto b_{irr}^{1/2}(1 - b_{irr})^k$ in the field region of $B > B_{F_p}^{max}$. The k value for the present samples is listed in Table IV. One can notice that the k value is

TABLE IV. The scaling parameters k in $f_p \propto b_{irr}^{0.5}(1 - b_{irr})^k$ are obtained from the data in the high-field region ($B_{F_p} < B < B_{irr}$).

Sample	parameter k
FSC	1.91 ± 0.05
MT1	2.09 ± 0.04
MT1F	1.86 ± 0.02
MT2	1.84 ± 0.03
MT3	1.68 ± 0.04

sample dependent and systematically decreases from 2.09 (MT1) to 1.68 (MT3) with increasing Nd422 content. Phenomenologically, the relation of $f_p - b_{irr}$ shifts from the catastrophic depinning type ($k=2$) to the avalanche depinning type ($k=1$) when the amount of Nd422 inclusions is increased. It is thus assumed that a combination of catastrophic depinning and avalanche depinning occurs in the higher-field region above $B_{F_p}^{max}$. Assuming that Nd123/Nd422 interface pinning become more dominant with increasing Nd422 content, the result indicates that interface pinning is effective pinning even in the high-field region, such that the samples with the larger amount of Nd422 inclusions show smaller k values in the $f_p - b_{irr}$ fitting curves.

The role of Nd422 inclusions in high-field regime is also proven by a different volume pinning force analysis. Recently, a general scaling formula to deduce the type of pinning regime was proposed by Jirsa and Púst.⁵⁷ They proposed that $f_p - b_{F_p}$ scaling is equivalent to the scaling of J_c normalized by the current density at the peak position, $J_c^{pk}(B_{J_c}^{pk})$ versus the reduced field $b_{J_c} = B/B_{J_c}^{pk}$:

$$J_c / J_c^{pk} = (b_{J_c}^{pk})^m \exp\{(m/n)[1 - (b_{J_c}^{pk})^n]\}. \quad (8)$$

The parameters m and n describe the pinning regime. Based on the analyses for numerous R123 samples from the literature, Jirsa and Púst found that Eq. (8) can describe the scaling properties with m kept to be unity and n being a variable parameter. For the volume pinning force, using the conditions $F_p(B_{F_p}^{max})/F_p^{max} = 1$ and $[dF_p(B)/dB] = 0$ at $B = B_{F_p}^{max}$, and noting that $B_{J_c}^{pk} \neq B_{F_p}^{max}$, Eq. (8) can be transformed to

$$B_{F_p}^{max} = B_{J_c}^{pk} [(m+1)/m]^{1/n} \quad (9)$$

and

$$f(b_{F_p}) = b_{F_p}^{m+1} \exp[(m+1)(1 - b_{F_p}^n)/n]. \quad (10)$$

For a comparative study among the samples, we conducted a fitting using Eq. (10). Here we note the fitting was unsuccessful for the data in the entire field region because of the large deviation in the low-field region. However, we found a fairly good scaling for the data above $B_{F_p}^{max}$, as shown in Fig. 6. Here we obtained $n = 2.52$ for the single crystal (FSC) and $n = 2.09$ for OCMG-processed Nd-Ba-Cu-O sample (MT3). It is clear that the n value decreases with increasing Nd422 content. A similar tendency has been reported in the previous papers.^{53,58} Since the ratio $B_{irr}/B_{F_p}^{max}$ increases with reducing n in Eq. (10), a large n value means that B_{irr} is the higher for the constant $B_{F_p}^{max}$ value. This shows that Nd422 addition is in fact effective in enhancing B_{irr} or the IL, which is supported by the results both in $J_c - B$ and $f_p - b_{irr}$ curves. Moreover, the experimental results also show that the $B_{F_p}^{max}$ value is slightly higher for the sample with more Nd422 inclusions, which implies that B_{irr} is increased with Nd422 addition.

C. The effect of Nd422 inclusion on the pinning property

The $B - T$ phase diagram in Y-Ba-Cu-O crystals has been extensively studied.^{35,37,38,59-63} Recently, the presence of

vortex liquid, Bragg glass, and a vortex glass phase have been clarified in pure Y-B-C-O single crystals.⁶⁴ These information will provide valuable suggestions on the vortex phase diagram in melt-processed samples. However, the vortex pinning mechanism in the melt-processed Nd-Ba-Cu-O sample is much more complicated. This is mainly attributed to the fact that the samples contains many kinds of defects. In fact, as we have shown above, interface pinning, $\Delta\kappa$ pinning, and point pinning are active at temperatures above 77 K. Their function and effectiveness will differ depending on many factors, such as their size, concentration, temperature, and magnetic field. Also, one has to take account of the fact that thermal activation will smear the efficiency of a given defect at a certain condition.

The CC model, which treats collective actions of several defects over a certain correlation length or volume, has been frequently applied in analyzing magnetic properties and the B - T phase diagram in many high-temperature superconductors, especially for a ‘‘clean’’ sample like a single crystal. Krusin-Elbaum *et al.*⁶¹ and Civale *et al.*⁶² studied magnetization curves and relaxation, and argued that the fishtail peak is related to a crossover from a single vortex pinning regime to a collective pinning regime. Later, many studies have been carried out based on CC theory to account for pinning properties in high-temperature superconductors.⁶⁵ However, the CC model cannot be directly applied to our OCMG-processed samples. First, ‘‘strong’’ pinning (Nd422 inclusions) active at high temperatures is not assumed in the CC theory. Second, plastic interaction between vortices is more important in this regime,⁶³ rather than elastic interaction, which is assumed in the CC model. Third, our samples contain various types of pinning centers, which makes it difficult to apply any single theoretical model to describe our experimental data in the entire temperature and field region. In this section, therefore, we focus on the function of Nd422 inclusions, which is the most effective pinning in OCMG-processed Nd-Ba-Cu-O.

Here, we show how the Nd422 inclusions affect the pinning mechanism in OCMG-processed Nd-Ba-Cu-O bulks, because little is known about the effect of nonsuperconducting inclusions on the B - T phase diagram nor the combined effect of several pinning centers. As we have described so far, the pinning regime can be classified into three regimes. The first regime is a low-field region where a combination of point pinning and interface pinning is active. The boundary between the first and second field regimes is $B_{J_c}^{defl}$, below which the $J_c \propto B^{\gamma-1}$ and $F_p \propto B^\gamma$ relation is fulfilled. The second region is an intermediate field region where $\Delta\kappa$ pinning becomes active and thus the fishtail in the J_c - B curve is observed. In this regime which is between $B_{J_c}^{defl}$ and $B_{F_p}^{max}$, the pinning force is not simply related to any determined pinning mechanism, i.e., both the interface pinning and $\Delta\kappa$ pinning are in function. Thus the J_c is influenced in a complex manner by various defects like nonsuperconducting precipitates, Nd-rich Nd123ss clusters, and point defect (oxygen deficiency). The third regime is between $B_{F_p}^{max}$ and B_{irr} , where f_p - b_{F_p} curves measured at various T above 77 K are well scaled onto a single master curve. This suggests that a temperature-independent pinning mechanism is dominant and $B_{F_p}^{max}$ is a crossover line in the B - T phase diagram.

TABLE V. The list of characteristics field.

Sample	$B_{J_c}^{defl}$ (T)	$B_{F_p}^{max}$ (T)	B_{irr} (T)
FSC	0.2±0.2	2.2±0.1	5.3±0.1
MT1	0.3±0.1	2.4±0.1	6.1±0.1
MT1F	0.5±0.1	2.6±0.1	6.6±0.1
MT2	0.6±0.1	2.8±0.1	7.0±0.1
MT3	0.6±0.1	3.0±0.1	7.1±0.1

The characteristic magnetic fields, $B_{J_c}^{defl}$, $B_{F_p}^{max}$, and B_{irr} at 77 K are listed in Table V. It is evident that the characteristic magnetic fields slightly shift to higher fields as Nd422 content (V_f/d value) is increased. This probably comes from the fact that Nd123/Nd422 interface pinning is active in the entire field region below B_{irr} ; the increase of volume pinning force by Nd123/Nd422 interface pinning results in the enhancement of $B_{J_c}^{defl}$, $B_{F_p}^{max}$, and B_{irr} .

There is a further point which needs to be clarified; the question is whether the magnitude of fishtail or the fishtail itself is affected by the presence of Nd422 inclusions. If two pinning centers can function simultaneously, the J_c - B curve may be expressed as a simple summation of two different contributions. Thus we separated the J_c - B curve into two components. We assume the first component gradually decays with B and finally reaches zero at B_{irr} . The second component is mainly active in an intermediate-field region where the fishtail effect is observed. The first and second component will represent the J_c - B curve attributed to interface pinning and $\Delta\kappa$ pinning, respectively. Here, we term the first and second components as the background critical current ($J_{c,bk}$) and the additional critical current (ΔJ_c), respectively, and $J_c(B) = J_{c,bk}(B) + \Delta J_c(B)$. Then we deduced the contribution from the first component assuming $J_{c,bk} = Ab_{irr}^p(1 - b_{irr})^q$ where A is a numerical constant, and p and q are fitting parameters. The scaling parameters used to deduce the background critical current density $J_{c,bk}$ are listed in Table VI. Here, we used the data at low fields ($B < 0.4$ T) and high fields ($B > 5$ T) where the contribution of the fishtail is supposed to be negligibly small.

The results of numerical calculation for MT1 and MT1F are plotted in Fig. 8. It is evident that the $J_{c,bk}$ curve fits well both at low and high fields. In addition, the $J_{c,bk}$ - B curve is similar to the field dependence of J_c observed in melt-processed Y-Ba-Cu-O bulk without the fishtail effect.^{8,35} On the other hand, the ΔJ_c - B curve, obtained from the relation

TABLE VI. The scaling parameters used to deduce the background critical current $J_{c,bk}$.

Sample	B_{irr}	$F_p \propto b_{irr}^p(1 - b_{irr})^q$ ($0 < B < 0.4$ T, 5.0 T $< B < B_{irr}$)		
		A	p	q
FSC	5.3	0.28	0.48	0.49
MT1	6.1	2.49	0.95	1.61
MT1F	6.6	3.83	0.81	1.45
MT2	7.0	1.59	0.73	1.17
MT3	7.1	0.99	0.60	0.91

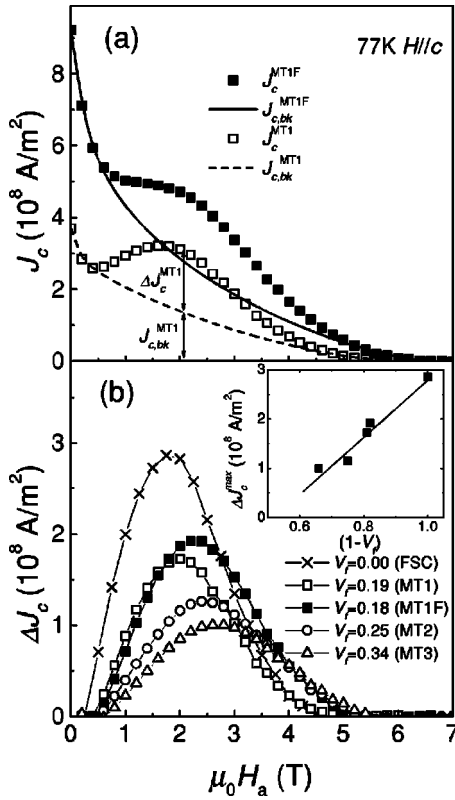


FIG. 8. Analysis of J_c - B property by separating it into two components: background critical current ($J_{c,bk}$) and additional critical current (ΔJ_c). (a) The relation between $J_{c,bk}$ - B and J_c - B at 77 K ($H||c$) for MT1F and MT1. The solid and dashed line correspond to the (numerically deduced) $J_{c,bk}$ value for MT1F and MT1, respectively, while filled and open squares correspond to the (measured) J_c value. (b) The ΔJ_c - B dependence for the samples studied here. Inset of (b): the relation between ΔJ_c^{max} and the cross-sectional area of the Nd123 matrix, where a good linear relation is recognized.

of $\Delta J_c = J_c - J_{c,bk}$, shows the maximum at an intermediate field, which is quite similar to the shape of the J_c - B curve in Nd123 single crystal. These results support the idea that the $J_{c,bk}$ - B curve and ΔJ_c - B curve represent the J_c contribution from the interface pinning and $\Delta \kappa$ pinning in the OCMG-processed Nd-Ba-Cu-O.

It has been generally believed that moderate concentration of nonsuperconducting inclusion (i.e., Nd422 inclusions) enhances the current in the low-field regime, whereas a much higher concentration of weakly interacting defects (i.e., Nd123ss) produces a fishtail peak in the medium field range.²⁴ In this point of view, a desirable improvement in J_c is to achieve a simple addition of both currents from a combination of both defect structures. However, it has been supposed difficult to introduce the two pinning simultaneously for the following reasons: one is the interference between the two pinning, and the other is whether or not the elementary pinning interaction sums up linearly to the global pinning force per volume.

Here, it is important to notice that the maximum ΔJ_c value ($\equiv \Delta J_c^{max}$) in MT1 and MT1F are nearly the same. This suggests ΔJ_c^{max} is proportional to the volume fraction of Nd123 matrix. In other words, overall J_c is a simple summation of $J_{c,bk}$ and ΔJ_c , and that $\Delta \kappa$ pinning can cofunction

with Nd123/Nd422 interface pinning without any significant interference. To confirm this assumption further, we also conducted the same analysis for FSC, MT2, and MT3, and found that ΔJ_c^{max} is almost proportional⁵ to the cross-sectional area of the Nd123 matrix [inset of Fig. 8(b)]. One should notice that the result provides very important suggestions on the pinning properties in Nd-Ba-Cu-O composites. First, ΔJ_c per Nd123 matrix is not affected by Nd422 addition. This supports the assumption that the fishtail peak is caused by the presence of Nd123ss clusters in the Nd123 matrix. Second, the overall J_c is a simple summation of $J_{c,bk}$ and ΔJ_c . This means J_c in the entire field region could be further enhanced by the introduction of strong interface pinning without decaying $\Delta \kappa$ pinning, although the ‘‘shape’’ of fishtail itself may be smeared or ‘‘washed away’’ due to the growth of $J_{c,bk}$. For example, Weber⁶⁶ and Chikumoto *et al.*⁶⁷ observed a complete disappearance of the fishtail peak in melt-processed Nd-Ba-Cu-O samples after introducing ‘‘strong’’ artificial pinning centers through neutron irradiation. This is probably due to the significant enhancement in background J_c , with low-field J_c near $2 \times 10^9 \text{ A/m}^2$ as compared to $1.5 \times 10^8 \text{ A/m}^2$ prior to irradiation. Third, the fishtail peak is related to the properties of elementary pinning centers^{11,50} in that a direct summation in pinning force can be recognized. It also suggests that $\Delta \kappa$ pinning is strong pinning in the sense that it enhances the J_c in the intermediate field region at elevated temperatures.

IV. CONCLUSION

We have performed a systematic study on the role of $\text{Nd}_4\text{Ba}_2\text{Cu}_2\text{O}_{10}$ (Nd422) nonsuperconducting particles for flux pinning in Nd-Ba-Cu-O bulk superconductors. We measured magnetic properties of several OCMG-processed Nd-Ba-Cu-O samples with different amount and size of Nd422 inclusions, together with a single crystal. Nd422 inclusions are found to act as the interface pinning which is the most effective and dominant at low fields and high temperatures. The pinning can be enhanced with increasing V_f/d either by increasing the amount of Nd422 (V_f) or by reducing the size (d). The pinning by Nd422 is quite similar to that of Y211 inclusions in Y-Ba-Cu-O. Nd422 addition is also found to be effective in enhancing the J_c and F_p even near B_{irr} .

There are three pinning regimes in the B - T phase diagram at elevated temperatures ($T \geq 77 \text{ K}$): a combination of point pinning and Nd123/Nd422 interface pinning below B^{defl} ; a combination of interface pinning and $\Delta \kappa$ pinning between B^{defl} and $B_{F_p}^{max}$; and interface pinning with a slight influence from $\Delta \kappa$ pinning between $B_{F_p}^{max}$ and B_{irr} , where a combination of catastrophic and avalanche depinning occurs. Nd422 addition shifted the boundary of the pinning regime to higher fields.

Overall J_c is almost a simple summation of the contributions of two independent J_c - B curves. One is a combination of pointlike pinning and Nd123/Nd422 interface pinning, in that J_c decreases with B . The other is $\Delta \kappa$ pinning mainly active in an intermediate-field region and is responsible for the fishtail in the J_c - B curve. These different pinning centers can act simultaneously. It is found that the magnitude of $\Delta \kappa$ pinning is proportional to the volume of the Nd123 matrix.

ACKNOWLEDGMENTS

This work was supported by the New Energy and Industrial Technology Development Organization (NEDO) as Collaborative Research and Development of Fundamental Technologies for Superconductivity Applications under the New Sunshine Program administered by the Agency of Industrial

Science and Technology (AIST) of the Ministry of International Trade and Industry (MITI) of Japan. The authors would like to thank Dr. H. S. Chauhan, Dr. H. Kojo, and Mr. K. Sawada for the sample preparation. Thanks are also due to Dr. S. I. Yoo, Dr. M. R. Koblishka, Dr. N. Sakai, and Mr. T. Higuchi for helpful discussions.

- ¹M. Murakami, *Melt Processed High Temperature Superconductors*, edited by M. Murakami (World Scientific, Singapore, 1993).
- ²M. Murakami, M. Morita, K. Doi, and K. Miyamoto, *Jpn. J. Appl. Phys.*, Part 1 **28**, 1189 (1989); S. Jin, T.H. Tiefel, R.C. Sherwood, M.E. Davis, R.B. van Dover, G.W. Kammlott, R.A. Fastnacht, and H.D. Keith, *Appl. Phys. Lett.* **52**, 2074 (1988); K. Salama, V. Selvamanicham, L. Gao, and K. Sun, *ibid.* **54**, 2352 (1989).
- ³M. Murakami, H. Fujimoto, S. Gotoh, K. Yamaguchi, N. Koshizuka, and S. Tanaka, *Physica C* **185-189**, 321 (1991).
- ⁴K. Salama, A.S. Parikh, and L. Woolf, *Appl. Phys. Lett.* **68**, 1993 (1996).
- ⁵S.I. Yoo and R.W. McCallum, *Physica C* **210**, 147 (1993).
- ⁶S.I. Yoo, N. Sakai, H. Takaichi, T. Higuchi, and M. Murakami, *Appl. Phys. Lett.* **65**, 633 (1994).
- ⁷M.J. Kramer, S.I. Yoo, R.W. McCallum, W.B. Yelon, H. Xie, and P. Allenspach, *Physica C* **219**, 145 (1994).
- ⁸M. Murakami, S.I. Yoo, T. Higuchi, N. Sakai, J. Weltz, N. Koshizuka, and S. Tanaka, *Jpn. J. Appl. Phys.*, Part 2 **33**, L715 (1994); M. Murakami, S.I. Yoo, T. Higuchi, N. Sakai, M. Watahiki, N. Koshizuka, and S. Tanaka, *Physica C* **235-240**, 2781 (1994).
- ⁹M. Murakami, N. Sakai, T. Higuchi, and S.I. Yoo, *Supercond. Sci. Technol.* **9**, 1015 (1996).
- ¹⁰M. Daeumling, J.M. Seuntjens, and D.C. Larbalestier, *Nature (London)* **346**, 332 (1990).
- ¹¹H.H. Wen and Z. Zhao, *Appl. Phys. Lett.* **68**, 856 (1996).
- ¹²H. K pfer, Th. Wolf, C. Lessing, A.A. Zhukov, X. Lancon, R. Meier-Hirmer, W. Schauer, and H. Wuhl, *Phys. Rev. B* **58**, 2886 (1998).
- ¹³A. Erb, J.-Y. Genoud, F. Marti, M. D umling, E. Walker, and R. Fl kiger, *J. Low Temp. Phys.* **105**, 1033 (1996); A. Erb, E. Walker, J.-Y. Genoud, and R. Fl kiger, *Physica C* **282-287**, 89 (1997).
- ¹⁴T. Egi, K. Kuroda, H. Unoki, and N. Koshizuka, *Appl. Phys. Lett.* **67**, 2406 (1995); T. Egi, J.G. Wen, K. Kuroda, H. Mori, H. Unoki, and N. Koshizuka, *Physica C* **270**, 223 (1996).
- ¹⁵W. Ting, T. Egi, R. Itti, K. Kuroda, N. Koshizuka, and S. Tanaka, *Jpn. J. Appl. Phys.*, Part 1 **35**, 4034 (1996); W. Ting, T. Egi, K. Kuroda, N. Koshizuka, and S. Tanaka, *Appl. Phys. Lett.* **70**, 770 (1997).
- ¹⁶W.A. Fietz and W.W. Webb, *Phys. Rev.* **178**, 657 (1969).
- ¹⁷E.J. Kramer, *J. Appl. Phys.* **44**, 1360 (1973).
- ¹⁸D. Dew-Hughes, *Philos. Mag.* **30**, 293 (1974).
- ¹⁹A.M. Campbell and J.E. Evetts, *Adv. Phys.* **21**, 199 (1972).
- ²⁰M.V. Feigel'man, V.B. Geshkenbein, and V.M. Vinokur, *Phys. Rev. B* **43**, 6263 (1991).
- ²¹G. Blatter, M.V. Feigel'man, V.B. Geshkenbein, A.I. Larkin, and V.M. Vinokur, *Rev. Mod. Phys.* **66**, 1125 (1994).
- ²²R. Griessen, H.H. Wen, A.J.J. van Dalen, B. Dam, J. Rector, H.G. Schnack, S. Libbrecht, E. Osquiguil, and Y. Bruynseraede, *Phys. Rev. Lett.* **72**, 1910 (1994).
- ²³N. Chikumoto, J. Yoshioka, M. Otsuka, N. Hayashi, and M. Murakami, *Physica C* **281**, 253 (1997).
- ²⁴Th. Wolf, A-C. Bornarel, H. K pfer, R. Meier-Hirmer, and B. Obst, *Phys. Rev. B* **56**, 6308 (1997).
- ²⁵N. Chikumoto, S. Ozawa, and M. Murakami, *Appl. Supercond.* **6**, 163 (1998).
- ²⁶H. Wu, M.J. Kramer, K.W. Dennis, and R.W. McCallum, *Appl. Phys. Lett.* **71**, 3572 (1997).
- ²⁷F. Sandiumenge, N. Vilalta, J. Rabier, and X. Obradors, *Appl. Phys. Lett.* **73**, 2660 (1998).
- ²⁸K. Sawada, S.I. Yoo, N. Sakai, T. Higuchi, and M. Murakami, in *4th Euro Ceramics*, edited by A. Barone, D. Fiorani, and A. Tampieri (Gruppo Editoriale Faenza Editrice, Faenza, 1995), Vol. 6, p. 293.
- ²⁹H. Kojo, S.I. Yoo, N. Sakai, and M. Murakami, *Superlattices Microstruct.* **21**, 37 (1997).
- ³⁰H.S. Chauhan and M. Murakami, *Mater. Sci. Eng., B* **56**, 48 (1999).
- ³¹N. Chikumoto, S. Ozawa, S.I. Yoo, N. Hayashi, and M. Murakami, *Physica C* **278**, 187 (1997).
- ³²K. Takita, H. Katoh, H. Akinaga, M. Nishino, T. Ishigaki, and H. Asano, *Jpn. J. Appl. Phys.*, Part 2 **27**, L57 (1988).
- ³³B.H.P. Weisinger, F.M. Sauerzopf, and H.W. Weber, *Physica C* **203**, 121 (1992).
- ³⁴P. Manuel, C. Aguillon, and S. Senoussi, *Physica C* **177**, 281 (1991); L.A. Dorosinskii, V.I. Nikitenko, A.A. Polyanskii, and V.K. Vlasko-Vlasov, *ibid.* **219**, 81 (1994).
- ³⁵T. Higuchi, S.I. Yoo, and M. Murakami, *Phys. Rev. B* **59**, 1514 (1999).
- ³⁶A.I. Larkin and Yu. N. Ovchinnikov, *J. Low Temp. Phys.* **34**, 409 (1979).
- ³⁷M.V. Feigel'man, V.B. Geshkenbein, A.I. Larkin, and V.M. Vinokur, *Phys. Rev. Lett.* **63**, 2303 (1989); M.V. Feigel'man and V.M. Vinokur, *Phys. Rev. B* **41**, 8986 (1990).
- ³⁸B. Mart nez, X. Obradors, A. Gou, V. Gomis, S. Pin l, J. Fontcuberta, and H. Van Tol, *Phys. Rev. B* **53**, 2797 (1996).
- ³⁹M. Murakami, S. Gotoh, N. Koshizuka, S. Tanaka, T. Matsushita, S. Kambe, and K. Kitazawa, *Cryogenics* **30**, 390 (1990).
- ⁴⁰M. Murakami, S. Gotoh, H. Fujimoto, K. Yamaguchi, N. Koshizuka, and S. Tanaka, *Supercond. Sci. Technol.* **4**, S43 (1991).
- ⁴¹M. Murakami, K. Yamaguchi, H. Fujimoto, N. Nakamura, T. Taguchi, N. Koshizuka, and S. Tanaka, *Cryogenics* **32**, 930 (1992).
- ⁴²R. Yu, F. Sandiumenge, B. Mart nez, N. Vilalta, and X. Obradors, *Appl. Phys. Lett.* **71**, 413 (1997).
- ⁴³M.R. Koblishka, A.J.J. van Dalen, T. Higuchi, K. Sawada, S.I. Yoo, and M. Murakami, *Phys. Rev. B* **54**, R6893 (1996); M.

- Jirsa, M.R. Koblischka, T. Higuchi, and M. Murakami, *ibid.* **58**, R14 771 (1998).
- ⁴⁴P.J. Kung, M.P. Maley, M.E. McHenry, J.O. Willis, M. Murakami, and S. Tanaka, *Phys. Rev. B* **48**, 13 922 (1993).
- ⁴⁵M. Muralidhar, M.R. Koblischka, T. Saitoh, and M. Murakami, *Supercond. Sci. Technol.* **11**, 1349 (1998); M. Muralidhar, M.R. Koblischka, and M. Murakami, *Physica C* **313**, 232 (1999).
- ⁴⁶K. Waki, T. Higuchi, S.I. Yoo, and M. Murakami, *Appl. Supercond.* **5**, 133 (1997).
- ⁴⁷C.C. Almasan, C.L. Seaman, Y. Dalichaouch, and M.B. Maple, *Physica C* **174**, 93 (1991).
- ⁴⁸Y. Dalichaouch, B.W. Lee, C.L. Seaman, J.T. Markert, and M.B. Maple, *Phys. Rev. Lett.* **64**, 599 (1990).
- ⁴⁹J.S. Satchell, R.G. Humphreys, N.G. Chow, J.A. Edwards, and M.J. Kane, *Nature (London)* **334**, 331 (1988); L. Civale, M.W. McElfresh, A.D. Marwick, F. Holtzberg, C. Feild, J.R. Thompson, and D.K. Christen, *Phys. Rev. B* **43**, 13 732 (1991); H. Yamasaki, K. Endo, S. Kosaka, M. Umeda, S. Yoshida, and K. Kajimura, *Phys. Rev. Lett.* **70**, 3331 (1993).
- ⁵⁰L. Klein, E.R. Yacoby, Y. Yeshurun, A. Erb, G. Müller-Vogt, V. Breit, and H. Wühl, *Phys. Rev. B* **49**, 4403 (1994).
- ⁵¹T. Matsushita, *Physica C* **205**, 289 (1993); N. Ihara and T. Matsushita, *ibid.* **257**, 223 (1996); M. Kiuchi, E.S. Otabe, T. Matsushita, T. Kato, T. Hikata, and K. Sato, *ibid.* **260**, 177 (1996).
- ⁵²T. Mochida, N. Chikumoto, and M. Murakami, *Appl. Supercond.* **6**, 217 (1998).
- ⁵³M.R. Koblischka, A.J.J. van Dalen, T. Higuchi, S.I. Yoo, and M. Murakami, *Phys. Rev. B* **58**, 2863 (1998).
- ⁵⁴O.B. Hyun, M. Yoshida, T. Kitamura, and I. Hirabayashi, *Physica C* **258**, 365 (1996).
- ⁵⁵T. Matsushita, M. Ito, A. Kikitsu, and Y. Miyamoto, *Phys. Rev. B* **33**, 3134 (1986).
- ⁵⁶T. Matsushita and H. Küpfer, *J. Appl. Phys.* **63**, 5048 (1988).
- ⁵⁷M. Jirsa and L. Püst, *Physica C* **291**, 17 (1997).
- ⁵⁸M.R. Koblischka, T. Higuchi, S.I. Yoo, and M. Murakami, *J. Appl. Phys.* **85**, 3241 (1999).
- ⁵⁹M.P.A. Fisher, *Phys. Rev. Lett.* **62**, 1415 (1989).
- ⁶⁰D.S. Fisher, M.P.A. Fisher, and D.A. Huse, *Phys. Rev. B* **43**, 130 (1991).
- ⁶¹L. Krusin-Elbaum, L. Civale, V.M. Vinokur, and F. Holtzberg, *Phys. Rev. Lett.* **69**, 2280 (1992).
- ⁶²L. Civale, L. Krusin-Elbaum, J.R. Thompson, and F. Holtzberg, *Phys. Rev. B* **50**, 7188 (1994).
- ⁶³Y. Abulafia, A. Shaulov, Y. Wolfus, R. Prozorov, L. Burlachkov, Y. Yeshurun, D. Majer, E. Zeldov, V.B. Geshkenbein, and V.M. Vinokur, *Phys. Rev. Lett.* **77**, 1596 (1996).
- ⁶⁴T. Nishizaki and N. Kobayashi, *Supercond. Sci. Technol.* **13**, 1 (2000), and references therein.
- ⁶⁵C. Hucho and M. Levy, *Phys. Rev. Lett.* **77**, 1370 (1996); R. Hiergeist and R. Hergt, *Phys. Rev. B* **55**, 3258 (1997); L. Burlachkov, D. Giller, and R. Prozorov, *ibid.* **58**, 15 067 (1998).
- ⁶⁶H.W. Weber, in *Proceedings of the 10th Anniversary HTS Workshop on Physics, Materials and Applications*, edited by B. Batlogg *et al.* (World Scientific, Singapore, 1996), p. 163.
- ⁶⁷N. Chikumoto, M. Konczykowski, T. Terai, and M. Murakami, *Supercond. Sci. Technol.* (to be published).